Pol. J. Environ. Stud. Vol. XX, No. X (XXXX), 1-19
DOI: *10.15244/pjoes/213364* ONLINE PUBLICATION DATE: 2026-02-09

Original Research

Spatiotemporal Patterns and Ecological Trade-offs of Open-pit Mining in Northwest China: A Remote Sensing Perspective on Environmentally Sustainable Development

Haihui Han[1,2,3], Xiaojuan Yan[1,2]*, Haojie Cai[1,2], Zhuan Zhang[1,2], Xiaoyan Chen[1,2], Yong Xu[1,2], Chendi Gao[1,2], Zhouyuan Zhang[4], Min Yang[5]**

[1]Xi'an Geological Survey Center of China Geological Survey / Northwest Center of Geological Technology Innovation, Xi'an 710119, China
[2]Key Laboratory for the Study of Focused Magmatism and Giant Ore Deposits of Magmatic Ore Deposits, Ministry of Natural Resources, Xi'an 710119, China
[3]Innovation Center for Engineering Technology of Intelligent Remote Sensing Monitoring of Natural Resources in the Upper-Middle Reaches of the Yellow River, Ministry of Natural Resources, Xi'an 710119, China
[4]Shaanxi Guangtai Project Management Consulting Co., Ltd, Xi'an 710075, China
[5]School of Resources Engineering, Xi'an University of Architecture and Technology, Xi'an 710055, China

Received: 3 June 2025
Accepted: 19 October 2025

Abstract

The rapid expansion of open-pit mining in Northwest China, driven by growing demands for energy and strategic minerals, poses significant challenges to environmental sustainability in arid and semi-arid ecosystems. Leveraging high-resolution remote sensing data (e.g., Gaofen-2/6, ZY-3), this study systematically analyzed the spatiotemporal patterns of 12,680 mining polygons across 3,253 approved open-pit mines in four northwestern provinces (Xinjiang, Qinghai, Gansu, and Ningxia) from 2021 to 2022. Results revealed a pronounced spatial clustering of mining activities, with 92% of the total mining area concentrated in Xinjiang and Qinghai. Non-metallic mineral extraction (potash, lithium, coal) dominated, accounting for 71.8% of the total footprint, while metallic mining showed localized impacts. Global Moran's I (0.156, $p<0.01$) and Getis-Ord Gi* analyses identified two high-intensity clusters in potassium-rich basins, demonstrating significant spatial autocorrelation. Desertification sensitivity assessments in key coal mining zones revealed that 55% of mining areas fell within high-sensitivity

*e-mail: hhaihui@mail.cgs.gov.cn
Tel.:13335397961
**e-mail: ymin@xauat.edu.cn
Tel.:13630287759

regions, correlating with post-2016 NDVI declines. Despite progress in avoiding protected areas (only 0.45% overlap), ecological trade-offs persisted-mining contributed 31% to Qinghai's GDP but degraded 12% of grasslands annually. Methodologically, manual interpretation achieved 95% accuracy but faced scalability limitations compared to automated machine learning approaches. The findings underscore the necessity of environmental, landscape-scale governance frameworks to address spillover effects between protected and high-density mining zones. We advocate integrating AI-enhanced monitoring and blockchain traceability to strengthen green mining practices, emphasizing that sustainable resource development in fragile ecosystems requires balancing economic priorities with spatially explicit ecological safeguards. This work provides a replicable model for reconciling mineral extraction with environmental conservation in global arid regions.

Keywords: open-pit mining, northwest China, remote sensing monitoring, spatial autocorrelation analysis, sustainable development

Introduction

The abundant mineral resources in the Northwest region are an important material foundation for ensuring the rapid development of China's economy and society [1]. Their extraction has a significant impact on regional economic and social development, environmental protection and management, and sustainable resource utilization [2]. The agricultural land conversion monitoring framework proposed by Worachairungreung et al. [3] demonstrates how advanced remote sensing technologies can systematically quantify human-land interactions in the context of resource development. The methodological advances showcased in the 30-year policy impact analysis by Rattanarat et al. [4] highlight the significant value of incorporating temporal dimensions into spatial monitoring frameworks. However, monitoring and understanding of the overall mining footprint remain limited. It is imperative to explore how to utilize Earth observation technology better to promptly and accurately assess the current spatial distribution of mining activities and their environmental impacts. Additionally, conducting regular and quantitative analyses and evaluations of the rationality of mining layout, the efficiency of intensive resource utilization, the effectiveness of ecological restoration and management, and the harmonious and green stability of mining areas is essential [5].

Remote sensing detection and monitoring are important means to quickly understand the current status of mineral resource development and changes in the geological environment of mines [6]. With the rapid development of remote sensing technology, high spatial resolution remote sensing data offer the combined advantages of macroscopic coverage, rapid acquisition, and synchronicity, and their application in mine monitoring is becoming increasingly widespread [7]. Especially in recent years, the number, spatial resolution, and monitoring frequency of domestic satellites have greatly improved, providing technical support for large-scale, high-precision monitoring and analysis of mining conditions [8]. In the past, many scholars have conducted related research using multi-source remote sensing data at the scale of typical mines or important mining areas in China, including the application of technical methods, monitoring of mining activities, and evaluation of the geological environment of mines [9]. There are also scholars who have conducted macro analyses of global mining development patterns [10]. However, there are currently few reports on the use of high-precision, high-frequency remote sensing monitoring to analyze the characteristics and patterns of mineral development at a regional scale. The author believes this may be related to several constraints, including high funding requirements, lengthy cycles, large volumes of data collection and processing, and difficulties in fully verifying the analysis results.

Since 2003, the China Geological Survey has organized its affiliated units to carry out experimental research on "Remote Sensing Dynamic Monitoring of Mineral Resource Development Status in five test areas, including the Huairou Gold Mine in Beijing [11]. In 2006, the China Geological Survey organized its affiliated units to carry out projects such as "Multi-Objective Remote Sensing Dynamic Monitoring of Mineral Resource Development in Important Metallogenic Belts and Mineral Concentration Areas", officially using remote sensing methods to monitor three targets: the status of mineral resource development, the mine environment, and the implementation of mineral resource planning [12]. Since 2010, the China Geological Survey has carried out pilot monitoring of key mines nationwide, and in 2011, it issued the "Technical Requirements for Remote Sensing Monitoring of Mineral Resource Development" as an industry standard [13]. Since 2021, the China Geological Survey has coordinated the nationwide remote sensing monitoring of mine development status [14]. The Xi'an Geological Survey Center has undertaken the public welfare survey project "Remote Sensing Monitoring of Mine Development and Ecological Restoration Status in Northwest China" (2021-2025) since 2021, one of whose goals is to continuously monitor the development and utilization of mineral resources (excluding oil and gas) in Xinjiang, Qinghai, Gansu, and Ningxia on a quarterly basis [15]. The mapping results have become an

important basis for the management departments to carry out mineral satellite image law enforcement work [16]. Although the monitoring data have shown significant results in management applications, the author believes that the understanding and comprehensive analysis of regional patterns based on high-precision observation data still need to be deepened, especially regarding the quantitative analysis of the mining development status in Northwest China.

In response to the aforementioned shortcomings, this study, based on recent work, conducted detailed research and analysis on the characteristics and patterns of approved open-pit mines under construction in the four provinces (regions) of Northwest China. Based on the mining rights approved by the management departments, this study utilized domestic satellite images from Gaofen-2, Gaofen-6, and Ziyuan-3 from 2021 and 2022 for remote sensing interpretation and analysis, generating the dataset with the largest number of polygons for open-pit mining land in the four provinces of Northwest China (V1.0) to date. This dataset accurately depicts the contour edges of mining land in the region, and the results have been verified by local management departments. On this basis, this paper applies spatial autocorrelation and other data analysis methods to further scientifically reveal the distribution patterns, mining dynamics, and geological environmental risks of typical sections of open-pit mines in Northwest China, aiming to provide a theoretical and practical basis for mining development management and green exploration implementation in the new round of prospecting breakthroughs.

Materials and Methods

Mineral Resources Overview of the Study Area

The Northwest region, located in the heart of the Eurasian continent, spans the Tethys and Paleo-Asian metallogenic domains. It has a complex tectonic evolution and diverse metallogenic processes, resulting in abundant energy and mineral resources, especially petroleum, coal, natural gas, nickel, gold, and potash [17]. According to previous statistics, the potential value of mineral resources in the five provinces of Northwest China is about 34 trillion yuan (accounting for 36% of the national total) [18, 19]. In terms of production, in 2020, the raw coal output was about 1.081 billion tons (accounting for 27% of the national total), crude oil output was 69.0567 million tons (accounting for 35% of the national total), natural gas output was 96.512 billion m^3 (accounting for 50% of the national total), the output of 10 nonferrous metals was 15.4384 million tons (accounting for 25% of the national total), and cement output was 798 million tons (accounting for 33% of the national total) [20]. From the perspective of resource exploration, since 1999, 16 large-scale mineral resource bases have been formed in the Northwest region, with major minerals including nickel, copper, lead-zinc, gold, molybdenum, iron, tungsten, and rare and rare-earth metals. A total of 25 super-large deposits and 140 large deposits have been discovered, and newly identified resource reserves have increased significantly, providing an important material foundation for the socio-economic development of the Northwest region [21].

Based on metallogenic regularity, the southern part of the Paleo-Asian metallogenic domain and the Qin-Qi-Kun metallogenic domain (including northern Xinjiang, northern Gansu, the southern edge of Xinjiang, and southern Qinghai and Shaanxi) mainly produce metallic minerals such as Hercynian marine volcanic iron deposits, skarn-type iron-copper deposits, porphyry copper deposits, magmatic segregation-type copper-nickel deposits, hydrothermal sedimentary lead-zinc deposits, and low-temperature hydrothermal gold deposits [22]. In the northern Qilian Mountains of Gansu, the main minerals are Caledonian massive sulfide copper-polymetallic deposits, skarn-type tungsten (molybdenum) deposits, and hydrothermal alteration rock-type copper deposits [23]. The northern section of the Sanjiang metallogenic belt in the Tethys metallogenic domain and parts of the Qinling area, which are superimposed by the Circum-Pacific metallogenic belt, are mainly affected by Indosinian-Yanshanian metallogenesis, producing porphyry copper (molybdenum) deposits and hydrothermal alteration rock-type gold deposits [24]. Nonmetallic minerals such as limestone for cement, dolomite for flux, refractory clay, fluorite, gypsum, construction sand and gravel, marble, and granite are widely distributed in the northwestern provinces [25], but potash and salt lake lithium are concentrated around the Qaidam Basin.

In terms of mining development, mining has become a pillar industry in the Northwest region, and its development has already reached a considerable scale. Statistics show that by the end of 1999, there were 13,429 mining enterprises in the Northwest region, of which state-owned and state-controlled enterprises accounted for 11% of the total number of mines, while non-state-owned enterprises accounted for 89%, and the ore output of non-state-owned enterprises accounted for 55% of the total [26]. According to incomplete statistics, the industrial output value of large-scale steel, nonferrous metals, building materials, and other mineral enterprises accounts for about 20% of the industrial output value of the Northwest region. Overall, most mining development and utilization in the northwest region is still in an extensive and inefficient stage, with low levels of deep processing, relatively short industrial chains, and relatively low added value of products and overall industrial benefits.

Data Processing and Interpretation Methodology

The remote sensing data employed in this study primarily consisted of high-resolution satellite imagery from domestic satellites such as GF-2, GF-6, and ZY-3,

with imagery captured predominantly between May and August of 2021 and 2022 [27-29]. The majority of the raw remote sensing data was distributed by the Natural Resources Aerogeophysical Survey and Remote Sensing Center of the China Geological Survey, while a minor portion was obtained through application and download from the Geological Cloud platform [30].

The NDVI data utilized in this paper were sourced from the Resource and Environment Science Data Platform [31]. The product name is the "Annual Maximum NDVI Dataset at 30 m Resolution for China", covering the period from 2000 to 2022. Data on soil moisture content used in the analysis were obtained from the National Tibetan Plateau Data Center, while geological disaster data were sourced from the Xi'an Geological Survey Center [32]. These raster data were resampled to a spatial resolution of 30 m. Additionally, the referenced land-use data were derived from the anonymized Third National Land Survey, and the boundaries of nature reserves and ecological function zones used for reference were internally distributed materials.

The remote sensing data were preprocessed using ENVI 5.6 software, which included radiometric calibration, data fusion, orthorectification, and image enhancement [33, 34]. The resulting preprocessed imagery, with a spatial resolution of 2 m, was suitable for monitoring open-pit mines. The interpretation was conducted using ArcGIS 10.8 software at a scale of 1:10,000 or larger. Changes between the two temporal datasets were analyzed through a combination of visual interpretation and machine-assisted recognition. This process identified and delineated various mining land-use types, such as mining sites, transfer yards, mining structures, and solid waste areas, providing information on their locations, quantities, and areas. Details of the specific types are presented in Table 1.

Given the inherent subjectivity of visual interpretation, the remote sensing interpretation results in this study were disseminated by the Ministry of Natural Resources to each county-level natural resources bureau. Professional technical personnel from these bureaus then conducted on-site verification of each individual patch using handheld GPS and BeiDou navigation devices for precise measurement and photographic documentation. The field survey data were uploaded through the national Land Cloud system, where patch boundaries and attributes were cross-checked against the existing database. Patches that passed on-site validation underwent a rigorous three-tier review process at the county, municipal, and provincial levels of the natural resources authorities before final submission, ultimately forming the validated and authoritative database.

Table 1. Types of mining occupations in open-pit mines.

Type code	Type	Type in legend
10	Stope	Stope
2A	Coal storage yard	Transit site
2B	Other ore stockpiles	Transit site
2C	Coal washing plant	Transit site
2D	Mineral processing plant	Transit site
2E	Processing pond	Transit site
3B	Tailings pond	Tailings pond
3C	Coal gangue pile	Solid waste
3D	Gangue pile	Solid waste
3E	Topsoil stockpile	Solid waste
3F	Internal waste dump	Solid waste
3G	External waste dump	Solid waste
4A	Production area	Mining building
4B	Residential area	Mining building
4C	Administrative area	Mining building
4D	Mine access road	Mining road
4E	Mine railway	Mining road
5A	Subsidence crater	Subsidence crater
GC	Restoration and rehabilitation project	Remediation area

Spatial Analysis Methods

Fishnet Analysis

To explore the distribution patterns and characteristics of open-pit mining land use in the four northwestern provinces (regions), we utilized the ArcGIS 10.8 Fishnet tool to partition the study area. The grid size was set to 100 km×100 km, a dimension that was chosen based on comprehensive considerations of spatial scale compatibility, statistical robustness, and practical application requirements within the study area. With county-level administrative units in the four northwestern provinces averaging approximately 11,000 km^2 in area, the 100 km grid size effectively corresponds to this jurisdictional scale while avoiding either excessive fragmentation (e.g., 50×50 km grids) that would compromise statistical validity or excessive aggregation (e.g., 200×200 km grids) that would obscure localized mining clusters. Spatial autocorrelation analysis (Moran's I and Getis-Ord Gi*) confirmed that this grid resolution maintains statistical significance (global Moran's I = 0.156, $p<0.01$) while being optimally compatible with the swath width of domestic satellite data (e.g., GF-6's 90 km coverage). This scale successfully captures both the aggregation patterns of small-scale mining operations (e.g., 547 mining polygons in Jingtai County, Gansu) and the spatial continuity of large mining districts (e.g., the 1,555 km^2 Lop Nur potash mine). Sensitivity analysis demonstrated

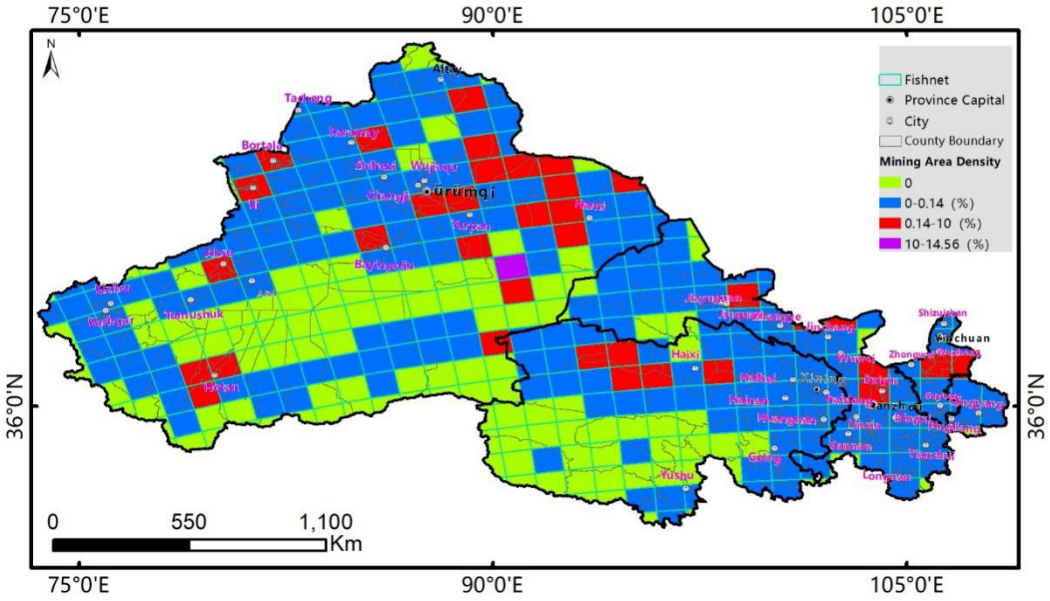

Fig. 1. Mine area density in four provinces in Northwest China.

that this resolution best identifies hotspot areas (e.g., the Shanshan-Ruoqiang region in Xinjiang and Dachaidan in Qinghai) while directly aligning with the 50-100 km monitoring units specified in China's Mineral Resources Planning (2021-2025), thereby ensuring both scientific rigor and policy relevance. Through this process, a total of 358 fishnet cells were generated (Fig. 1), with an average area of 8,239 km^2 per cell.

Moran's I Index

Moran's I was employed in this study to evaluate spatial autocorrelation, which quantifies whether observations within a geographic region exhibit interdependence and characterizes the strength and directionality of such spatial associations [35]. Moran's I is categorized into two forms: the Global Moran's I, which detects spatial autocorrelation across the entire study area, and the Local Moran's I, which identifies localized spatial patterns [35]. A statistically significant Global Moran's I (deviating from zero) indicates a nonrandom spatial distribution of data points at the global scale [36]. The Local Moran's I, conversely, assesses spatial autocorrelation at specific locations and their neighboring regions, facilitating the detection of localized clusters such as hotspots (aggregations of high values), coldspots (aggregations of low values), or spatial outliers [36]. The mathematical formulation of Moran's I integrates a spatial weight matrix (W = [wij]) and standardized covariance between variables. Its core equation is expressed as:

$$I = \frac{n}{\sum_{i=1}^{n}\sum_{j=1}^{n} w_{ij}} \cdot \frac{\sum_{i=1}^{n}\sum_{j=1}^{n} w_{ij}(X_i - \bar{X})(x_j - \bar{X})}{\sum_{i=1}^{n}(X_i - \bar{X})^2}$$

where n denotes the sample size, w_{ij} represents the spatial weight between observations i and j, X_i and X_j are observed values, and $\bar{X}$ is the mean of the variable.

The interpretation of Moran's I follows these criteria:

I>0: Positive spatial autocorrelation, reflecting clustering of similar values.

I<0: Negative spatial autocorrelation, indicating dispersion of dissimilar values.

I≈0: Spatial randomness, implying no statistically significant spatial pattern.

*Hotspot Analysis (Getis-Ord G$_i$)**

This study employed hotspot analysis (Getis-Ord G_i)* to identify spatial clustering patterns in mining development data, elucidating regions exhibiting statistically significant clusters of high values (hotspots) or low values (coldspots) [37]. The G_i statistic calculates a z-score for each spatial unit within the dataset, quantifying the likelihood of significant high- or low-value clustering around its location [37].

The G_i* statistic is expressed as:

$$G_i^* = \frac{\sum_j w_{ij}x_j - \bar{X}\sum_j w_{ij}}{S\sqrt{\frac{n\sum_j w_{ij}^2 - \left(\sum_j w_{ij}\right)^2}{n-1}}}$$

where x_j is the observed value at spatial unit j; $\bar{X}$ is the global mean of the dataset; S is the global standard deviation; w_{ij} is the spatial weight matrix, typically defined by distance decay or adjacency relationships; and n is the total number of spatial units.

The G_i* statistic is interpreted as a standardized z-score, where the magnitude and direction of the value indicate spatial clustering significance: a positive

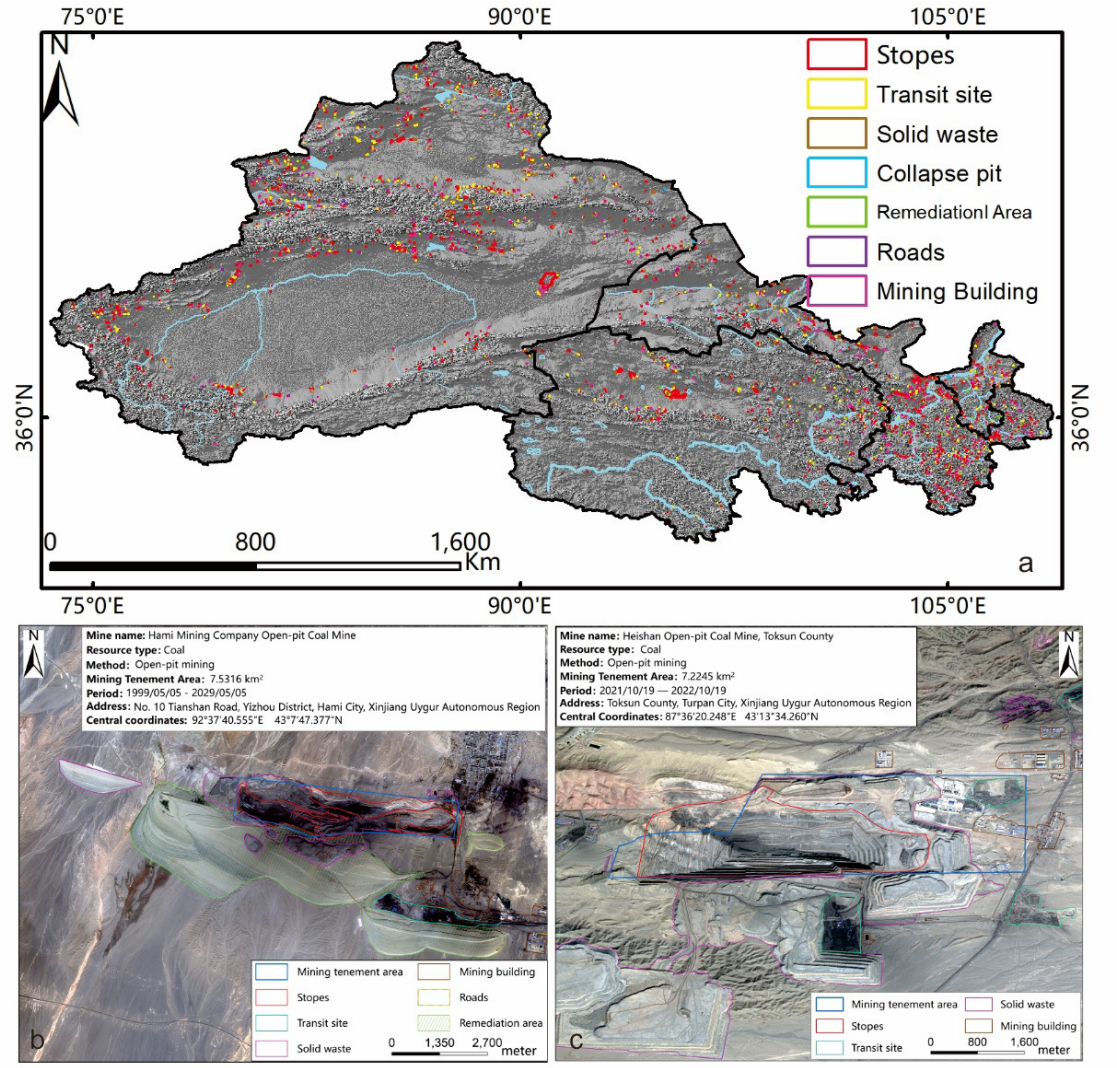

Fig. 2. Mining footprint of open-pit mines in four provinces in Northwest China.

z-score ($G_i* > 0$) denotes a hotspot (aggregation of high values), with increasing values reflecting stronger statistical significance, while a negative z-score ($G_i* < 0$) signifies a coldspot (aggregation of low values), where more negative values correspond to greater confidence in low-value clustering [38]. Statistical significance is typically assessed using predefined thresholds, aligning with conventional hypothesis-testing frameworks to categorize hotspots and coldspots into discrete confidence tiers.

Results and Discussion

Spatiotemporal Monitoring of Mining-Induced Land Disturbance in Open-Pit Mining Operations

The distribution of monitored patches in the four northwestern provinces (regions) is illustrated in Fig. 2. The monitoring results reveal that in 2022, a total of 3,253 approved and operational open-pit mines across these regions encompassed 12,680 polygonal mining patches, covering an area of 4,581.04 km^2, with an arithmetic mean of 0.36 km^2 per patch (total perimeter: 16,579.2 km; average perimeter: 1.31 km per patch). As shown in Fig. 1, while the common features of these mines include (but are not limited to) mining sites or pits, waste rock piles, mineral processing areas, and production/office facilities, they exhibit significant variability in spatial form and scale, such as distribution clustering and patch size. Among the patch types, mining sites are the most prevalent. Detailed characteristics of these mining patches, categorized by province and primary land-use type, are summarized in Table 2.

The distribution of patches across the four provinces (regions) shows a high degree of geographical connectivity, yet the patch distribution varies significantly. Approximately 54% of the patches are located in Xinjiang, 28% in Gansu, 12% in Qinghai, and only 6% in Ningxia. Notably, Xinjiang and Qinghai account for over 90% of the total patch area (Table 3). Fig. 3 highlights the top 10 county-level administrative regions with the highest number of open-pit mining

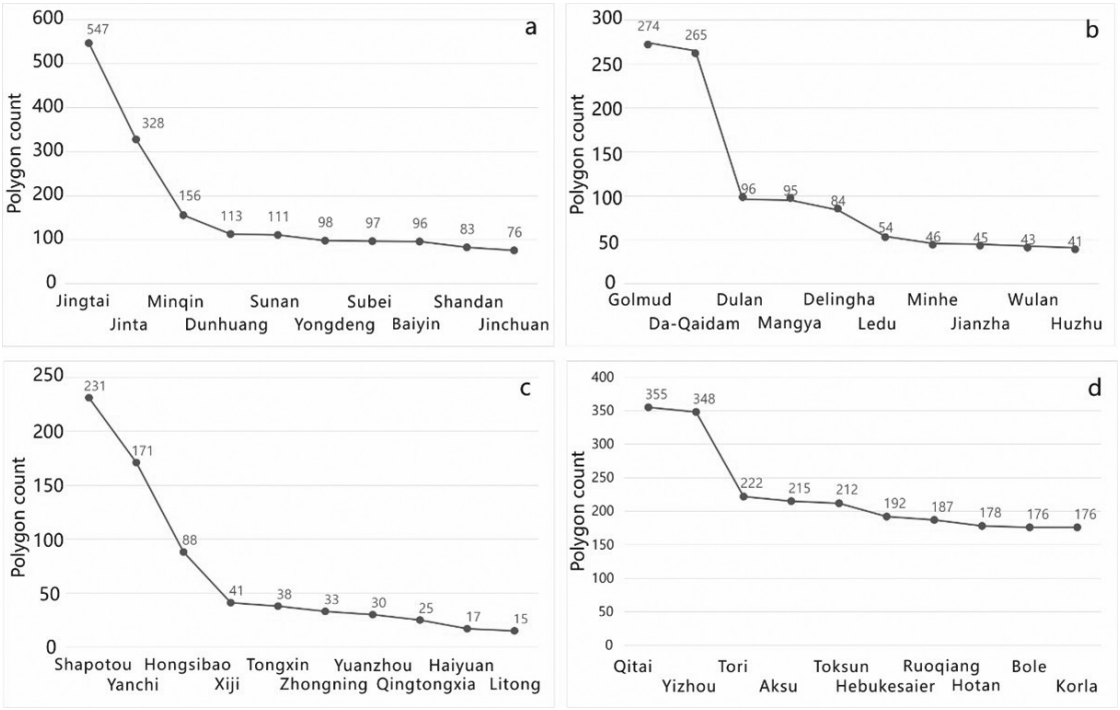

Fig. 3. Top 10 counties in terms of the number of mining polygons by provinces and regions. a) Counties from Gansu Province; b) Counties from Qinghai Province; c) Counties from Ningxia Hui Autonomous Region; d) Counties from Xinjiang Uygur Autonomous Region.

Table 2. Quantitative characteristics of mining polygons.

Provinces	Polygon count	Area (km^2)	Mean area (km^2/province)	Standard deviation (km^2/ province)	
Gansu	3577	270.11	0.08	0.38	This study
Qinghai	1530	1386.55	0.91	10.74	
Ningxia	729	52.11	0.07	0.21	
Xinjiang	6844	2872.27	0.42	19.32	
Four Northwestern Provinces (Regions)	12680	4581.04	0.36	14.68	
China	29348	7887.85	0.27	1.59	Reference
Four Northwestern Provinces (Regions) of China	2432	1437.39	0.59	4.71	
USA	6053	8499.04	1.4	5.45	
Russia	4659	8675.45	1.86	5.72	
Australia	4046	5319.70	1.31	4.74	
Indonesia	2117	3689.83	1.74	10.22	
South Africa	1984	3021.75	1.52	4.45	
Ukraine	1931	1348.92	0.7	7.56	
Other Countries	24410	27142.84	1.50		

land-use patches: Jingtai County (547 patches), Qitai County (355 patches), Yizhou District (348 patches), Jinta County (328 patches), Golmud City (274 patches), Dachaidan Administrative Committee (265 patches), Shapotou District (231 patches), Tuoli County (222 patches), Aksu City (215 patches), and Toksun County (212 patches). At the provincial level, the counties (districts) with the most patches are Qitai County in Xinjiang (coal, sand, and metal mines), Jingtai County in Gansu (coal, etc.), Golmud City in Qinghai (potash

Table 3. Area of occupation types of mining patches by province.

Polygon type	Gansu	Qinghai	Ningxia	Xinjiang	Total
Grass	72.07	261.83	35.82	170.35	540.07
Farmland	18.5	1.11	8.25	13.8	41.66
Industrial and Mining Storage Land	71.09	369.9	2.6	253.46	697.05
Forest Land	46.79	25.45	2.13	24.92	99.29
Other Land	53.95	176.72	2.32	2255.34	2488.33
Water Areas and Hydraulic Facilities	5.78	551.54	0	144.38	701.7
Garden Land	1.93	0	0.99	10.02	12.94
Total	270.11	1386.55	52.11	2872.27	4581.04

salt, etc.), and Shapotou District in Ningxia (coal, iron ore, etc.).

The analysis of mining types based on patch distribution (Figs 4 and 5) reveals that the socio-economic development of the northwestern region heavily relies on potash, lithium, coal, construction minerals, and metals such as iron, copper, and gold. Among these, potash occupies the largest area (2,670.13 km^2), followed by lithium (418.13 km^2) and coal (297.82 km^2). In terms of patch count, construction sand dominates, with 3,696 patches covering 297.53 km^2. Overall, the scale of non-metallic mineral resource extraction surpasses that of metallic minerals. Previous studies categorize major global mining countries into high mineral demand nations (e.g., China, India, and the United States) and high mineral export nations (e.g., Australia, Canada, South Africa, and Russia). The mining activities in the four northwestern provinces align with this pattern. For instance, construction materials like sand and granite are extensively consumed for infrastructure projects, while coal remains a critical resource for power and heating. Additionally, potash, lithium, iron, copper, and gold are indispensable for advancing agriculture and high-tech industries in recent years.

The analysis of land-use types occupied by the patches (Table 4) indicates that the primary land use in the northwestern region is bare land, saline-alkali land, and other unused land (2,488.33 km^2), followed by water bodies and water conservancy facilities (701.70 km^2), industrial and mining storage land (697.05 km^2), grassland (540.07 km^2), forest land (99.29 km^2), cultivated land (41.66 km^2), and garden land (12.94 km^2). Among these, Qinghai occupies the largest area of water bodies

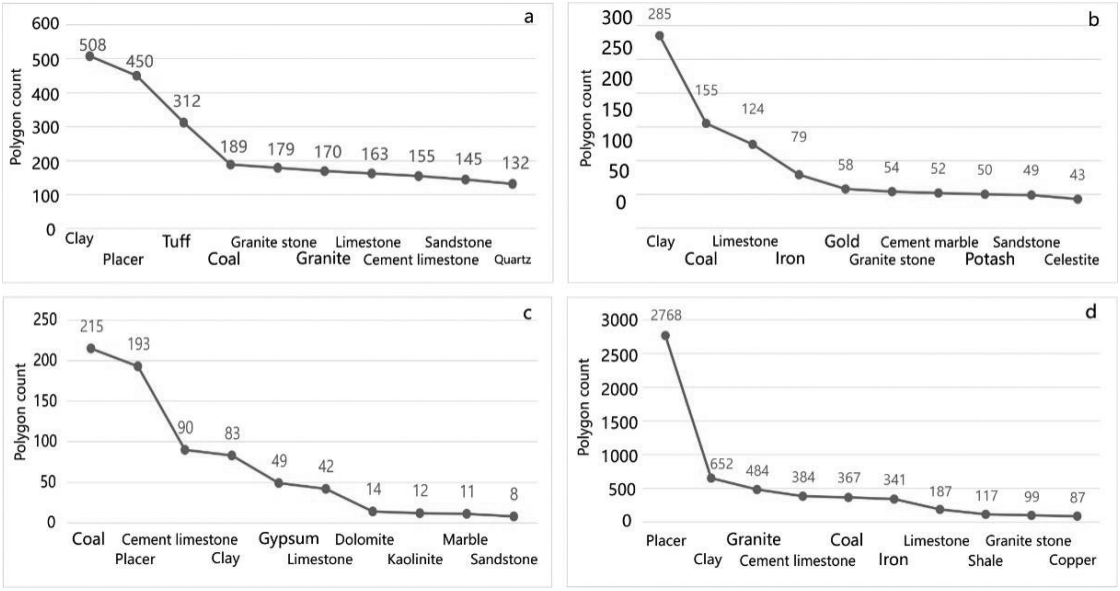

Fig. 4. Top 10 minerals in terms of the number of mining polygons by provinces and regions. a) Counties from Gansu Province; b) Counties from Qinghai Province; c) Counties from Ningxia Hui Autonomous Region; d) Counties from Xinjiang Uygur Autonomous Region.

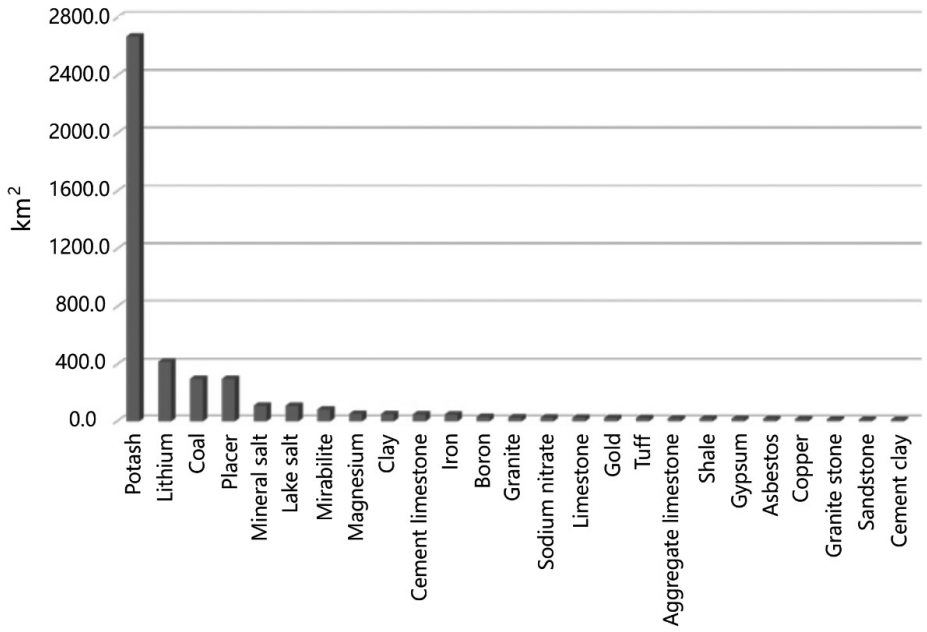

Contribution chart of the cumulative area of mines.

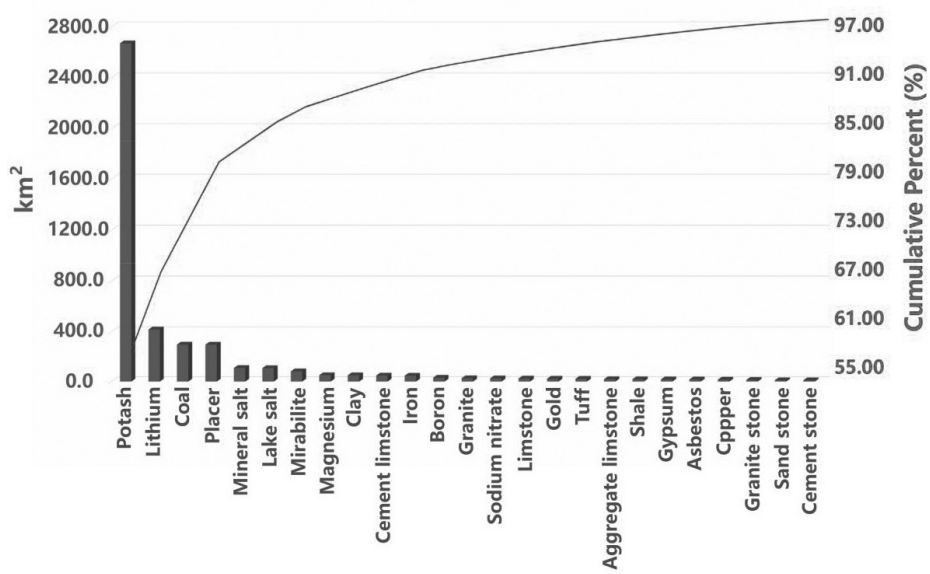

Fig. 5. Top 25 (area > 10 km^2) minerals in terms of the number of mining patches in four provinces.

and water conservancy facilities, Xinjiang occupies the most unused land, while Gansu and Ningxia occupy the most grassland. Regarding the overlap between patches and nature reserves (Table 5), 40 patches are distributed across 7 nature reserves, covering a total area of 20.84 km² and accounting for 0.45% of the total mining patch area. Of these, 28 patches are in Gansu, 7 in Ningxia, and 5 in Xinjiang. Additionally, the overlap between patches and ecological functional zones (Table 6) shows that although 8,202 patches (64.7% of the total) are located within 4 designated ecological functional zones, they only account for 25.2% of the total area. Ranked by patch count, the windbreak and sand-fixation zone contain the most patches (n=3,448, 385.39 km^2), followed by the soil conservation zone (n=2,111, 104.52 km^2), biodiversity zone (n=1,452, 556.97 km^2), and water conservation zone (n=1,191, 106.87 km^2). These results reflect that recent mining development in the northwestern region has placed greater emphasis on ecological protection and coordination. Approved mining areas have largely avoided nature reserves and key ecological zones, demonstrating a positive trend toward sustainable development and the construction of green mines in the region.

Table 4. Number and area of mining patches in nature reserves by province.

Provinces	Names of the protection areas	Polygon count	Area (km^2)
Gansu	Qilian Mountains National Nature Reserve	4	0.13
	Liancheng National Nature Reserve	21	0.96
	Xinglong Mountains National Nature Reserve	1	0.16
	Zhangye Heihe Wetland National Nature Reserve	2	0.24
Ningxia	Lingwu Baihitai National Nature Reserve	1	0.18
	Ningxia Helan Mountains National Nature Reserve	6	3.22
Xinjiang	Lop Nur Wild Camel National Nature Reserve	5	15.95
Total		40	20.84

Table 5. Number and area of mining patches in ecologically functional zones by province.

	Windbreak and Sand-fixation Zone		Biodiversity Conservation Area		Water Source Conservation Area		Soil Conservation Area	
	Polygon count	Area (km^2)	Polygon count	Area (km^2)	Polygon count	Area (km_2)	Polygon count	Area (km^2)
Gansu	1391	143.89	273	15.17	295	18.75	1371	69.59
Qinghai	480	72.58	282	24.12	86	3.26	314	12.61
Ningxia	528	34.52	11	1.40	14	5.19	132	8.18
Xinjiang	1049	134.40	886	516.28	796	79.67	294	14.14
Total	3448	385.39	1452	556.97	1191	106.87	2111	104.52

Table 6. Graded assignment of sensitivity factors for desertification.

Evaluation Factor	High Sensitivity	Relatively High Sensitivity	Moderate Sensitivity	Low Sensitivity
Soil Moisture Content (m^3/m^3)	<0.2	0.2~0.28	0.28~0.35	≥0.35
Evapotranspiration (mm/month)	≥200	130~200	80~130	<80
Annual Precipitation (mm/year)	<200	200~300	300~400	≥400
Average Wind Speed (m/s)	≥4.7	3.6~4.7	2.8~3.6	<2.8
Soil Sand Content (%)	≥70%	40%~70%	20%~40%	<20%
Soil Silt Content (%)	≥33%	22%~33%	5%~22%	<5%
Soil Clay Content (%)	<8%	8%~19%	19%~24%	≥24%
Soil Erosion Intensity	Severe	Moderate	Mild	Negligible
Slope Gradient (°)	≥25	10~25	5~15	0-5
Geohazard Susceptibility	High Susceptibility	Moderate Susceptibility	Low Susceptibility	Non-Susceptibility
Multi-year NDVI Mean Value	<0.2	0.2~0.4	0.4~0.6	≥0.6
NDVI Change Trend	<-0.12	-0.12~ -0.17	-0.17~0.0025	≥0.0025
Mining Development Land Occupation	Forest and Grassland	Agricultural Land	Unused Land	Construction Land
Graded Assignment	4	3	2	1

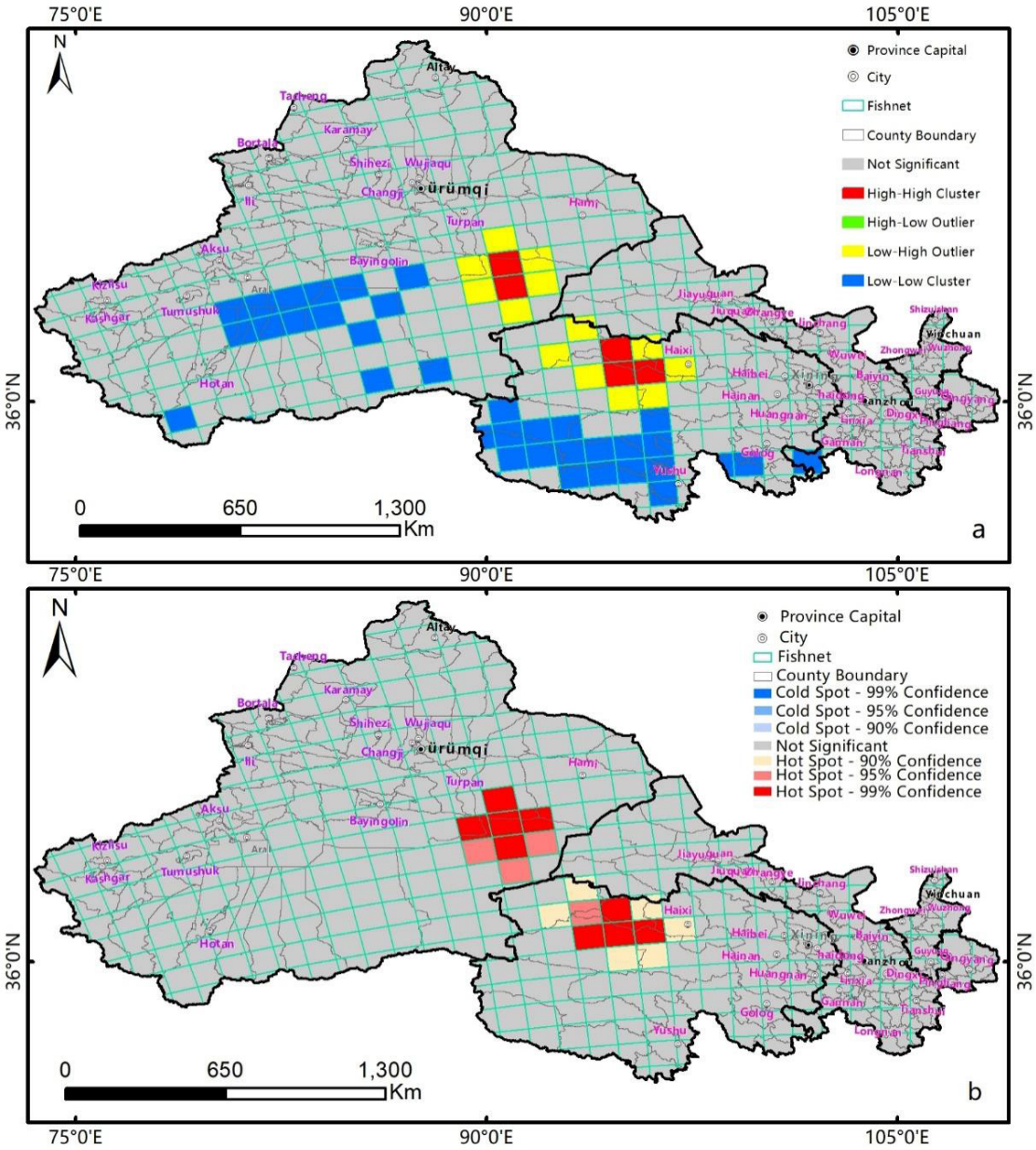

Fig. 6. Spatial heterogeneity of mine areas in four provinces in Northwest China. a) Clustering and Outlier Analysis; b) Hot spot analysis.

Spatial Distribution Characteristics of Mining-Induced Land Disturbance in Open-Pit Mining Development

The spatial analysis reveals that 12,680 mining patches were mapped into 225 out of the 358 fishnet cells, with mining density per cell ranging from 0 to 14.56% and an average of 0.14%. Cells with higher-than-average mining density are predominantly located in Xinjiang, particularly north of the Tianshan Mountains, including Urumqi and surrounding areas such as Changji, Turpan, Hami, and Fuyun County in Altay. In southern Xinjiang, higher densities are only observed in Aksu and Hotan. In Qinghai, high-density areas are mainly concentrated in the Qaidam Basin, while in Gansu, they are found in Baiyin and Jinchang. In Ningxia, high-density areas are primarily distributed in Wuzhong. Overall, higher-density mining areas are predominantly located around inland sedimentary basins, which may be attributed to regional metallogenic characteristics, mineral deposit scale, population, industrial development, and proximity to roads and railways. In contrast, regions such as southern Qinghai, the Qilian Mountains, and southern Xinjiang, which are at higher elevations, exhibit nearly zero mining density, likely due to recent environmental protection measures restricting mining and exploration. This reflects the government's increasing focus on balancing mining activities with ecological conservation.

To further elucidate the spatial heterogeneity characteristics of land occupation by open-pit mining development, this study conducted a global spatial

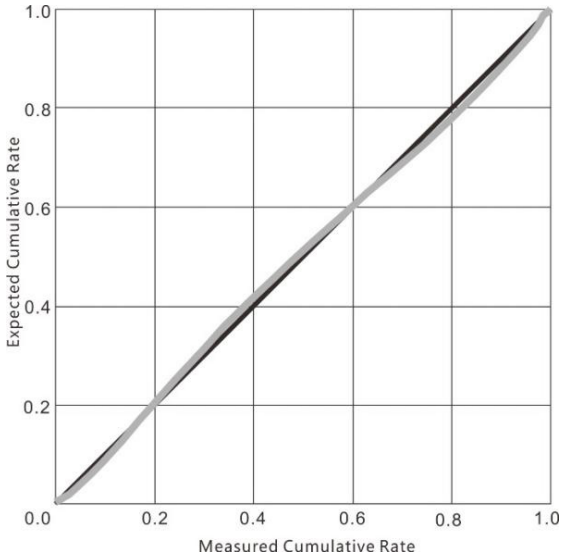

Fig. 7. Test for normal distribution of patch areas.

autocorrelation analysis of mining density. The Global Moran's I index yielded a positive value (0.156), with a relatively high Z-score (5.752) and a low P-value (0.0), indicating a significant positive spatial correlation in the distribution of open-pit mining development. The Getis-Ord General G analysis also showed a positive Z-score (5.76) and a P-value of 0, suggesting significant clustering of high values in the global distribution of mining development. To explore whether this pattern holds at the local level, a local spatial analysis was performed, as illustrated in Fig. 6. The Anselin Local Moran's analysis revealed that 82.39% of the area in the four provinces (regions) exhibited no clustering behavior (NS), while 1.70% of the area showed high-high clustering (HH). The proportions of high-low (HL) and low-low (LL) clustering anomalies were 4.41% and 11.5%, respectively. The Getis-Ord Gi* hotspot analysis identified two high-hotspot regions (with confidence levels greater than 90%), covering approximately 6.44% of the area. One hotspot is located at the junction of Shanshan County, Ruoqiang County, and Yuli County in Xinjiang, and the other is situated at the intersection of Dachaidan, Mangya, Golmud, and Dulan in Qinghai. Both regions are concentrated areas for potash mining. Both global and local spatial correlation analyses indicate that open-pit mining development in the four northwestern provinces (regions) exhibits significant regional tendencies, with large-scale mining activities (characterized by large patch areas) being relatively concentrated and showing a high-high clustering trend.

The scale variability of mining areas in the four northwestern provinces (regions) is considerable, with the smallest patch (mining roads) covering an area of less than 10 m^2, while the largest patch (potash mining) spans up to 1,555 km^2. The standard deviation of the polygon areas is 14.68 km^2. Normality tests on the data revealed that, on the log-normal P-P plot, the 12,680 sample points form an approximately straight diagonal line (Fig. 7), indicating that the frequency distribution of patch areas follows a log-normal distribution. Consequently, the geometric mean is more appropriate for representing the average land occupation of each mining feature (polygon). The calculated geometric mean is 0.024 km^2. The number of mining areas varies significantly across different scales, showing an overall logarithmic upward trend (Fig. 8a)). This trend is particularly pronounced in the range of 0-0.1 km^2. Analysis shows that 47.9% of all polygons have areas less than 0.024 km^2, while 81.6% of the regions have areas below 0.1 km^2. Additionally, 91% of the regions have areas less than 0.2 km^2, and 98.2% of the regions have areas below 1 km^2.

Although the number of medium- and large-sized mines (defined in this study as medium-sized with areas of 10-50 km^2 and large-sized with areas >50 km^2) is significantly smaller (totaling 26, with 17 medium-sized and 9 large-sized), the scale of these mines still strongly influences the total land occupation area of the 12,680 mining polygons. Statistical results (Fig. 8b)) show that regions with mining areas >10 km^2 account for 71.8% of the total polygon area, while those >50 km^2, >100 km^2, and >1000 km^2 account for 63.5%, 58.6%, and 34% of the total polygon area, respectively. When ranked by the number of medium- and large-sized mining polygons (areas >10 km^2), the order is Qinghai (16) > Xinjiang (9) > Gansu (1). A total of nine non-metallic minerals are produced from these sites, with the largest mining area being the Luobupo potash mine in Ruoqiang County, Xinjiang. By mineral type, potash is the most abundant

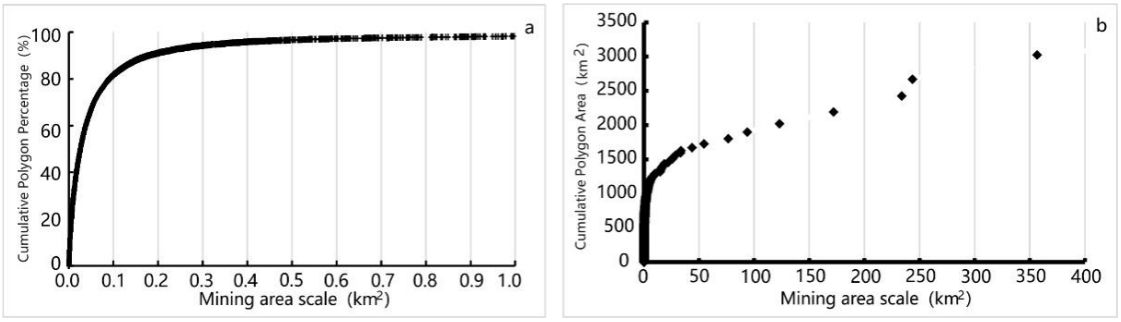

Fig. 8. Distribution of mining patches by size. a) is the multi-scale quantification of mining polygons in mineral resource extraction areas; b) is the multi-scale areal assessment of mining polygons in resource extraction areas.

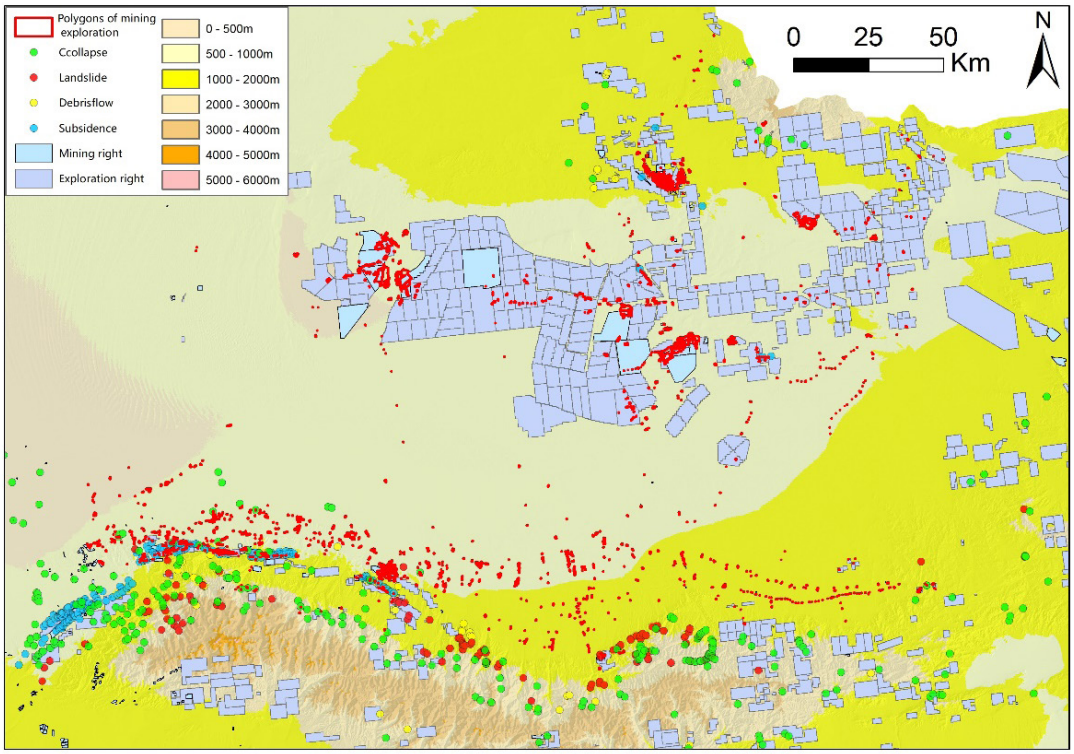

Fig. 9. Location of Demonstration Area.

(n=10, 2,608.6 km^2), concentrated in three regions: Golmud and Dulan in Qinghai, and Ruoqiang in Xinjiang. This is followed by rock salt (n=2, 105.2 km^2), lake salt (n=2, 41.5 km^2), mirabilite (n=2, 36.7 km^2), coal (n=2, 31.9 km^2), boron ore (n=1, 23.4 km^2), sodium nitrate (n=1, 16.8 km^2), and magnesium salt (n=1, 15.3 km^2). Although mineral supply is dominated by large mines, small-scale mining (<10 km^2) still accounts for approximately one-third (about 30%) of the total land use area for mining in the northwestern regions.

Desertification Sensitivity Analysis in Typical Mining Areas

Remote sensing monitoring of mining development and utilization in the four northwestern provinces (regions) conducted by our research team in 2022 revealed that the number of mining patches (including both legal and suspected illegal activities) in Qitai County and adjacent areas along the northern slope of the Tianshan Mountains in Xinjiang ranks among the highest in the northwestern regions. However, this area is located within the desert ecological zone in the Junggar Basin, raising concerns about whether mining activities may impact the ecological environment, particularly in terms of desertification. To address this question, we selected a demonstration area for desertification-sensitivity analysis and evaluation.

The demonstration area (as shown in Fig. 9) includes Fukang City, Jimsar County, Qitai County, and Mulei Kazakh Autonomous County, covering a total area of 47,431.37 km^2. This area encompasses the concentrated mining zones of the Beishan Coal Mine in Qitai County and the Wugong Coal Mine in Fukang City. A total of 4,477 mining patches (covering 218.90 km^2) are distributed within this region, among which 672 patches (153.86 km^2) are associated with open-pit mining. These patches occupy 124.89 km^2 of unused land, 46.74 km^2 of grassland, 32.27 km^2 of construction land (including 29.22 km^2 of mining land), 7.51 km^2 of forest land, 4.22 km^2 of agricultural land, and 3.27 km^2 of water bodies. Given the extensive study area, the use of NDVI data with 250-meter or 500-meter spatial resolution may be insufficient to accurately capture the ecological impacts of mining development, as many affected patches are relatively small. While employing higher-resolution data (e.g., 30-meter or finer) could improve detection, it would also substantially increase processing demands and analytical complexity. Therefore, this study focused on conducting long-term NDVI analysis specifically in the Fukang coal mining area in Xinjiang, as a representative case.

By analyzing the change trend of NDVI from 2000 to 2022, it was found that the areas with decreasing NDVI were mainly concentrated in the southern part of the region. The areas with increasing NDVI were mainly the newly cultivated land in the central part (with a relatively regular shape), and there were no significant change trends in other areas (Fig. 10). By analyzing the annual changes of NDVI (with a precision of 30 m) at different regional scales in the demonstration area from 2000 to 2022, it was found that the patterns of change

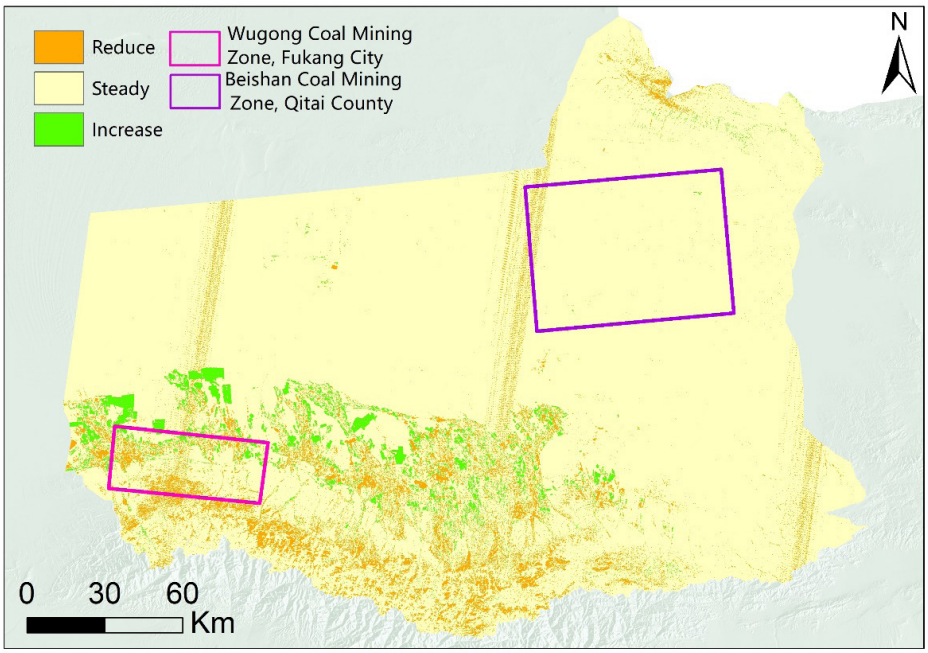

Fig. 10. Trends in NDVI.

at each scale were generally consistent, and there were two obvious change stages. As shown in Fig. 11, before 2016, NDVI generally showed a slow upward trend, and it decreased sharply after 2016. Although the NDVI value in the mining plot area was very low, the cliff-like decline indicated that the impact of human activities was still significant. It can be inferred that large-scale mine exploitation in this area began in 2016.

At the regional scale, this study integrated monitoring results with multi-element datasets, employing graded assignment and spatial hierarchical analysis methods to assess the impacts of mining development on regional desertification sensitivity. The evaluation framework incorporated two additional factors: mining development footprint and NDVI trend, with other contributing factors detailed in Table 6. Threshold determination for factor grading combined the natural-breaks method and empirical expert judgment. As shown in Fig. 12, the analysis results demonstrate good consistency with the existing ecological functional zoning outcomes, revealing high desertification sensitivity in two key mining districts. Notably, numerous mining and exploration rights have been approved in these sensitive areas, necessitating heightened emphasis on green exploration practices and mine-environmental restoration during subsequent mineral resource investigations and extraction activities.

Using the natural-breaks method, the final sensitivity values were classified into four levels: high (>34), relatively high (31-34), moderate (28-31), and low (22-28). Among 4,477 mining parcels, the low desertification sensitivity zones covered 10.31 km^2 (5.1% of the total area), moderate-sensitivity zones 22.23 km^2 (11%), relatively high-sensitivity zones 58.33 km^2 (28.9%), and high-sensitivity zones 110.87 km^2 (55%), as shown in Fig. 13. Although this analysis presents limitations, including variations in data precision across multiple factors and potential inaccuracies in the selection and assignment of certain evaluation indicators, the assessment results remain generally objective, demonstrating that mining activities exert measurable impacts on local desertification processes. It is

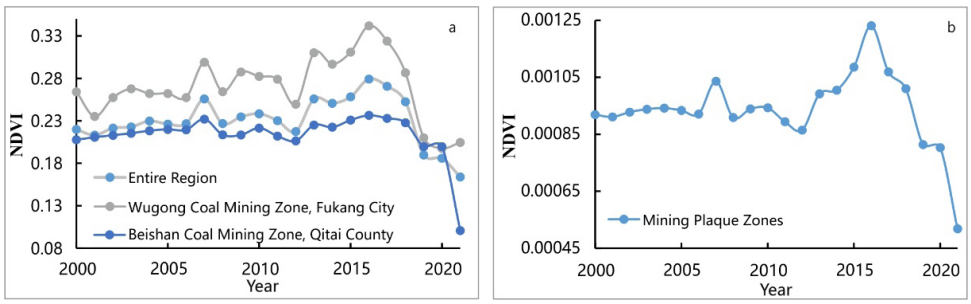

Fig. 11. Annual changes in NDVI at different regional scales in the demonstration area. a) NDVI dynamics across mining districts; b) vegetation index variation in mining polygons.

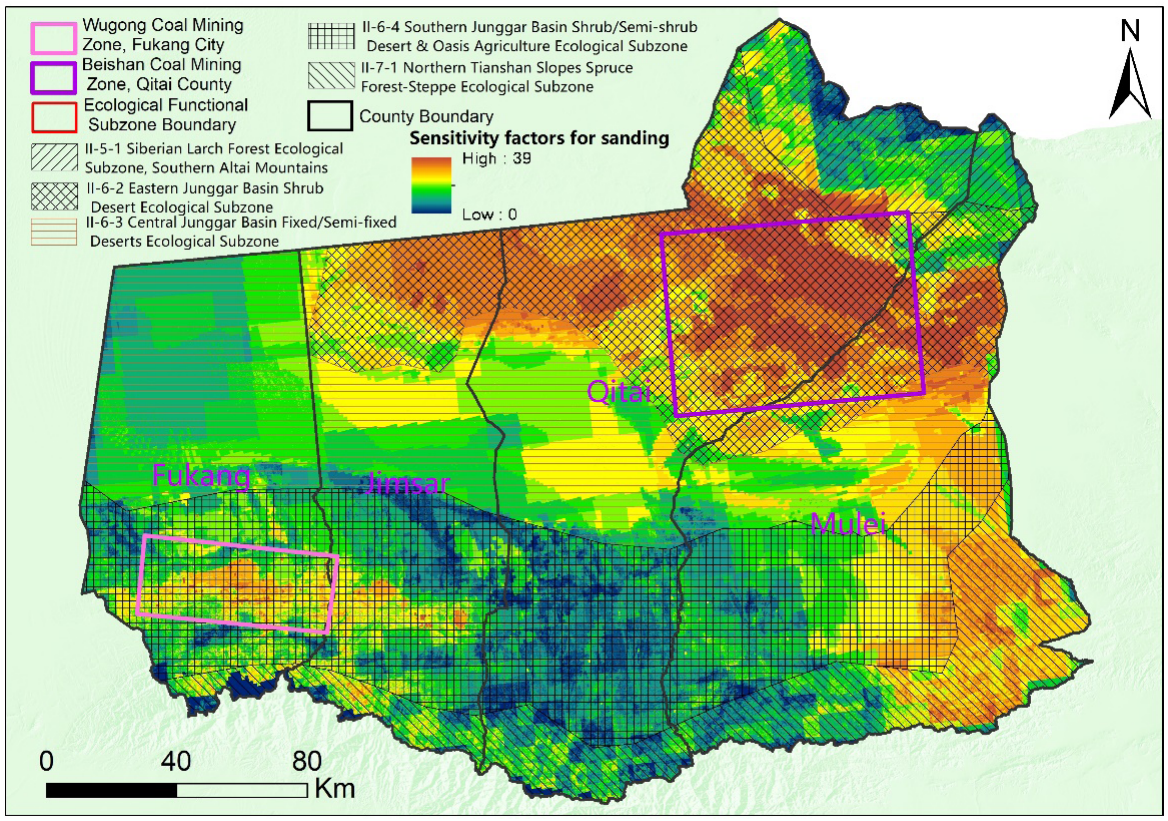

Fig. 12. Desertification sensitivity map of the demonstration area.

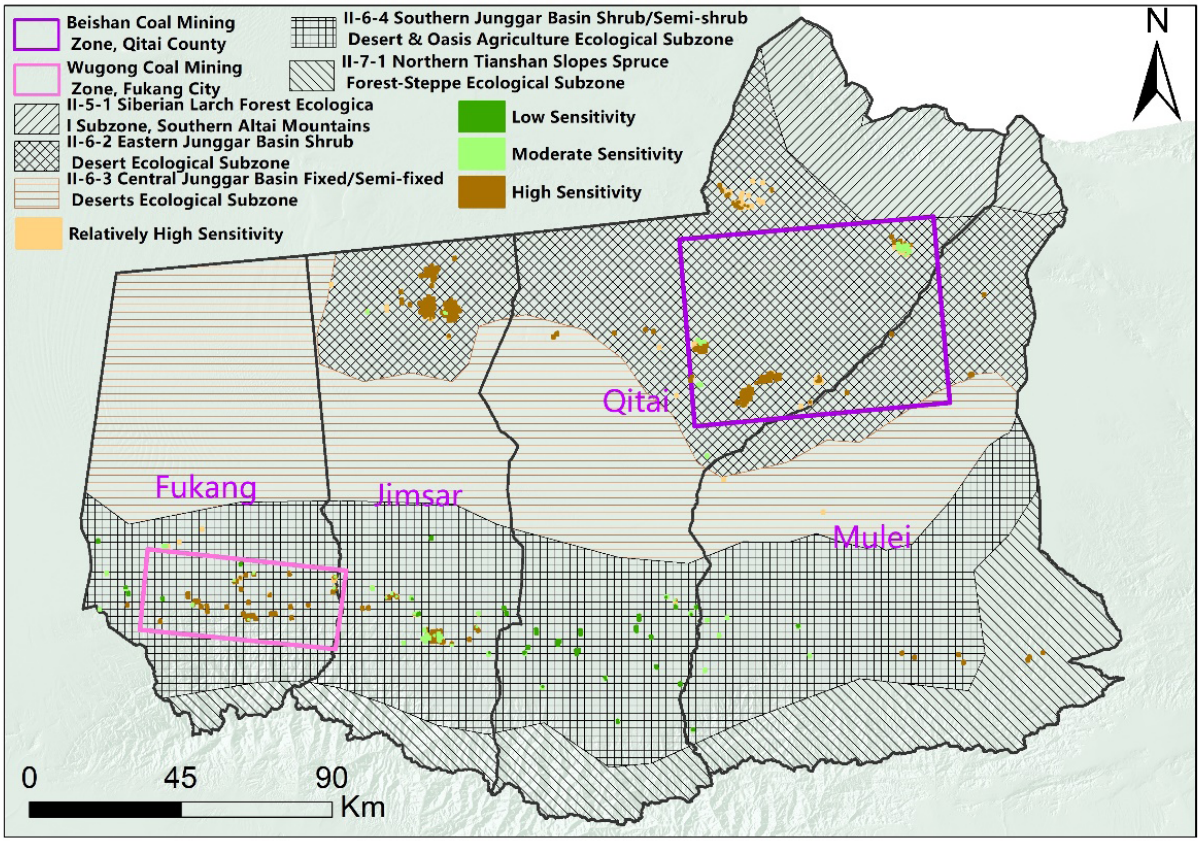

Fig. 13. Desertification sensitivity grading map for mining areas.

recommended that subsequent mineral rights allocation prioritize scientific rigor and rational planning, while efforts should be intensified to advance green-mine construction initiatives.

Global and Regional Patterns of Mining Impacts

The dominance of non-metallic mineral extraction (e.g., potash, coal, lithium) in China's northwestern provinces reflects a broader global trend where non-metallic mining operations account for a disproportionately large share of the total mining footprint compared to their economic contribution. Maus et al. quantified this phenomenon at a planetary scale, revealing that non-metallic mining accounts for 62% of global mining footprints despite generating only 38% of mineral-related GDP [39, 40]. Our findings align with their observations but further highlight regional specificities: in arid ecosystems like the Qaidam Basin, clustered mining activities (>70% coverage by medium-large mines) amplify habitat fragmentation – a critical threat to desert-adapted species. This contrasts with Tang et al.'s global database, which identified metallic mining (e.g., copper, gold) as the primary driver of biodiversity loss in tropical rainforests [41, 42]. Such biome-dependent impacts underscore Sonter et al.'s argument that mining threats must be evaluated through spatially explicit ecological lenses rather than universal metrics [43, 44].

The imperative for spatially differentiated approaches extends to policy. Strict mining restrictions implemented in ecologically sensitive zones (e.g., Qilian Mountains, Three-River Source) demonstrate the potential of targeted interventions to mitigate localized degradation [45]. However, the success of these measures depends on enforcement consistency – a challenge documented by Petropoulos et al. in their 23-year remote sensing analysis of Greek mines [46]. Their work revealed that while legislation reduced illegal mining by 40% post-2000, rehabilitation rates remained below 15% due to inadequate monitoring [47]. In northwestern China, the juxtaposition of strictly protected areas (e.g., Qilian Mountains, Three-River Source) and high-density mining zones (e.g., Qaidam Basin) epitomizes a "patchwork governance" dilemma: protective measures concentrated in specific zones may inadvertently displace or intensify extractive pressures onto ecologically vulnerable adjacent lands. This displacement can lead to spatial spillover effects, where environmental degradation (e.g., habitat loss, pollution, altered hydrology) originating in mining zones impacts bordering protected areas. Addressing these cumulative, cross-boundary impacts demands the landscape-scale planning frameworks championed by Sonter et al. [48, 49], moving beyond fragmented administrative units to manage ecological processes holistically.

Methodological Advancements and Limitations

Our manual interpretation approach achieved spatial classification accuracy comparable to Vasuki et al.'s 95% overall accuracy achieved with machine learning for mine boundary delineation [47]. While human analysts can discern subtle spectral variations in high-resolution imagery – particularly for non-metallic deposits like coal, which Mukherjee et al. showed have distinct SWIR-band signatures – the process is time-intensive and subjective [48]. A key limitation of manual methods is evident in tasks requiring temporal analysis, such as differentiating active mines from rehabilitated areas using Landsat time series. This process is laborious. In contrast, Vasuki et al. successfully automated this distinction using random forest algorithms, achieving 89% accuracy in identifying land cover change trajectories over time [47]. Our exclusion of underground mining activities, which account for 34% of China's coal production (National Bureau of Statistics, 2023), introduces systemic underestimation biases – a limitation also acknowledged in Maus et al.'s Global Surface Mining Database [40, 49].

The rapid expansion of mining into dispersed, biodiverse areas – projected by Yu et al. to increase by 300% in Asia by 2040 – demands more dynamic monitoring solutions [50]. Integrating Mukherjee et al.'s SWIR-based index with Yu et al.'s multi-sensor framework (Landsat-MODIS-DMSP/OLS) could address seasonal and scale-related challenges [48, 50]. For example, MODIS VI products (250 m resolution) enable monthly vegetation health assessments around mining sites, while DMSP/OLS nightlight data (1 km resolution) help detect unauthorized operations through energy-use patterns. Nevertheless, as Tang et al. rightly cautioned, an overreliance on satellite observations carries inherent risks of missing critical impacts that occur below the canopy or ground surface, are too spatially fine-grained, or involve subsurface processes (e.g., groundwater contamination, soil micro-pollution, localized habitat degradation) [41]. Therefore, robust monitoring frameworks must integrate satellite-based approaches with targeted ground surveys and in situ sensor networks to capture these hidden dimensions of mining impact.

Ecological and Socioeconomic Trade-offs

The vegetation suppression observed in desert mining zones exemplifies the direct terrestrial pathway of mining impacts described by Sonter et al. [43]. In hyper-arid regions, where plant communities rely on cryptic soil seed banks, even limited surface disturbance can trigger irreversible ecological shifts. This contrasts with the Qilian Mountains' alpine meadows, where enforced mining bans allowed 22% vegetation recovery between 2010-2020 (this study) – a success paralleling Australia's Darling Range bauxite mines, where Vasuki et al. measured 18% annual rehabilitation rates using

Landsat time series [47]. However, economic trade-offs persist: mining contributes 31% of GDP in Qinghai Province but degrades 12% of its grassland ecosystems annually. Balancing these competing demands necessitates implementing a structured approach, such as Sonter et al.'s "mitigation hierarchy" [43]. This framework prioritizes: first, avoiding impacts on the most sensitive areas; second, minimizing operational footprints where avoidance is not possible; third, restoring degraded sites during and after operations; and finally, offsetting any significant residual impacts that cannot be fully mitigated through earlier steps.

The regional mining-clustering phenomenon (e.g., Qaidam's high-high clusters) mirrors global patterns of resource-driven urbanization but poses unique governance challenges. As Tang et al. demonstrated, mining hubs often become enclaves of environmental risk, with 78% of global tailings dams located within 5 km of freshwater sources [41]. In northwestern China, the concentration of lithium mines – critical for renewable energy technologies – exemplifies the "green paradox", where sustainable infrastructure depends on ecologically intensive extraction. Resolving this tension requires comprehensive life-cycle assessments that quantify the net environmental and socioeconomic trade-offs. Integrating Yu et al.'s remote sensing indicators of ecological impact [50] with socioeconomic metrics – such as job creation, local revenue generation versus health costs, ecosystem service loss, and long-term remediation liabilities – would provide a holistic basis for evaluating the true sustainability of "critical" mineral extraction in fragile regions, a critical gap identified in our study.

Policy Implications and Technological Synergies

The effectiveness of mining bans in high-altitude protected areas validates Petropoulos et al.'s advocacy of spatially targeted regulations [46]. However, static protected boundaries may fail to accommodate climate-driven biome shifts – a critical concern given that 60% of China's mining regions face rising aridity (IPCC, 2023). Dynamic zoning systems, informed by real-time satellite monitoring and predictive modeling, could enhance adaptability. A practical application would be integrating our high-resolution mining-footprint dataset with Sonter et al.'s spatially explicit biodiversity impact models [43] to conduct scenario-based spatial planning. This would allow policymakers to identify future mineral extraction zones that minimize conflicts with projected critical habitats and ecological corridors under different climate and development scenarios.

Technological synergies offer transformative potential: Combining Mukherjee et al.'s spectral indices with deep learning architectures (e.g., convolutional neural networks) could automate mine detection at 90% + accuracy while reducing processing time by 80% (vs. manual methods) [48]; Blockchain traceability: Linking satellite-derived land-use maps with mineral supply chains (as proposed by Tang et al.) would enforce accountability for rehabilitation commitments [41]; Community science: Engaging local stakeholders in ground-truthing, as trialed by Maus et al. in the Congo's coltan mines, enhances data granularity while fostering environmental stewardship [40].

Conclusions

(1) Through comprehensive high-resolution remote sensing monitoring, it was found that 3,253 approved open-pit mines under construction in the four northwestern provinces (regions) involve a total of 12,680 mining polygons. These are primarily distributed in Xinjiang and Qinghai, with their polygon counts and area proportions reaching 66% and 92%, respectively. Among the mined minerals, potash, lithium, coal, construction materials, and metallic minerals such as iron, copper, and gold are mined at relatively large scales. However, overall, the scale of non-metallic mineral resource development exceeds that of metallic minerals.

(2) Spatial correlation analysis reveals that open-pit mining development in the four northwestern provinces (regions) exhibits a significant high-high clustering trend. High-density mining areas are predominantly located around inland sedimentary basins, with two high-hotspot regions identified as concentrated potash mining zones. The number of mining areas varies significantly across scales, showing an overall logarithmic upward trend. Although medium- and large-sized mines are few in number, they account for 71.8% of the total area, indicating that mineral supply is likely dominated by medium- and large-sized mines.

(3) Desertification sensitivity analysis in typical coal mining areas indicates that mining activities have a measurable impact on desertification in desert ecological zones. Therefore, it is recommended that future mineral rights allocation emphasize more scientific and rational planning, while simultaneously strengthening efforts to promote green mining practices.

(4) This study primarily relied on visual interpretation and field verification for remote sensing monitoring, resulting in a lengthy data extraction and analysis cycle. The next step will involve integrating more measured spectral data and artificial intelligence technologies to improve polygon extraction methods. This will enable long-term monitoring and analysis of mining development and environmental changes.

Acknowledgments

We are thankful to the Innovation Center for Engineering Technology of Intelligent Remote Sensing Monitoring of Natural Resources in the Upper-Middle Reaches of the Yellow River, and the Xi'an Geological Survey Center of China Geological Survey

for their contributions to this research. This research was funded by the Key Research and Development Program of Shaanxi (Program No. 2023-GHZD-38), the National Natural Science Foundation of China (grant No. 42272342), the High-Resolution Project of the National Defense Science, Technology, and Industry Administration (91-Y50G32-9001-22/23), the Project of Shaanxi Province Land Engineering Construction Group (No. DJNY2024-56), and natural Science Basic Research Program of Shaanxi (Program No.2024JC-YBQN-0315). The APC was supported by the Geological Survey Foundation of China Geological Survey (grant No. DD20211393 and DD20230106). The authors would like to thank the reviewers and editors for their helpful and constructive comments on this manuscript.

Conflicts of Interest

The authors declare no conflicts of interest.

References

1. ZHAI M., HU R., WANG Y., JIANG S., WANG R., LI J., CHEN H., YANG Z., LÜ Q., QI T., SHI X., LI Y., LIU J., LI Z., ZHU X. Mineral resource science in China: review and perspective. Geography and Sustainability. **2** (2), 107, **2021**.
2. LIANG R., TANG P., XIONG G., LIU Z., YU D. A review on sustainable development of geological exploration technology and risk management. Recent Patents on Engineering, **15** (1), 45, **2021**.
3. WORACHAIRUNGREUNG M., KULPANICH N., THANAKUNWUTTHIROT K., HEMWAN P. Monitoring agricultural land loss by analyzing changes in land use and land cover. Emerging Science Journal. **8** (2), 687, **2024**.
4. RATTANARAT J., JAROENSUTASINEE K., JAROENSUTASINEE M., SPARROW E.B. Government policy influence on land use and land cover changes: a 30-year analysis. Emerging Science Journal. **8** (5), 1783, **2024**.
5. VAN DER MEER F.D., VAN DER WERFF H.M.A., VAN RUITENBEEK F.J.A., HECKER C.A., BAKKER W.H., NOOMEN M.F., VAN DER MEIJDE M., CARRANZA E.J.M. Multi- and hyperspectral geological remote sensing: A review. International Journal of Applied Earth Observation and Geoinformation. **14** (1), 112, **2012**.
6. BISHOP C., RIVARD B., DE SOUZA FILHO C.R., VAN DER MEER F.D. Geological remote sensing. International Journal of Applied Earth Observation and Geoinformation. **64**, 267, **2018**.
7. WANG R., YAN B., LI M., DONG S., SUN Y., WANG B. Remote sensing interpretation of important ore-controlling geological units in Hongshan region of Gansu Province using GF-1 image and its application. Remote Sensing for Land and Resources. **30** (2), 162, **2018**.
8. SONG W., SONG W., GU H., LI F. Progress in the remote sensing monitoring of the ecological environment in mining areas. International Journal of Environmental Research and Public Health. **17** (6), 1846, **2020**.
9. HONG F., HE G., WANG G., ZHANG Z., PENG Y. Monitoring of land cover and vegetation changes in Juhugeng coal mining area based on multi-source remote sensing data. Remote Sensing. **15** (13), 3439, **2023**.
10. DENG X., GUI X., HE S., WANG C., LI Z., WANG Z., SONG M., YANG Q., ZHANG A., CHEN J. Research progress and prospect on development geography. Journal of Geographical Sciences. **31**, 437, **2021**.
11. CHEN B., LI Z., DONG F. Analysis of ore-controlling structure in the Qifengcha-Detiangou gold deposit, Huairou County, Beijing. Acta Geologica Sinica-English Edition. **75** (1), 94, **2001**.
12. TAGWAI M.G., JIMOH O.A., SHEHU S.A., ZABIDI H. Application of GIS and remote sensing in mineral exploration: current and future perspectives. World Journal of Engineering. **21** (3), 487, **2024**.
13. QIANG J. Study of remote sensing monitoring concerning geological environment of major metallogenic belt and mining concentrations in Shaanxi Province. Northwest Geology. **46** (3), 203, **2013**.
14. LIU H., JIANG Y., MISA R., GAO J., XIA M., PREUSSE A., SROKA A., JIANG Y. Ecological environment changes of mining areas around Nansi lake with remote sensing monitoring. Environmental Science and Pollution Research. **28**, 44152, **2021**.
15. HAN H., LI J., YI H. Application and prospect of remote sensing technology in geological survey of Northwest China. Northwest China. **55** (3), 155, **2022**.
16. IVANOVA Y.N., IVANOV K.S., BONDAREVA M.K., IVANOV I.G., ZHUKOV A.O. Using Unmanned Aerial Vehicles for Search and Prediction of Ore Mineralization. Izvestiya, Atmospheric and Oceanic Physics. **57** (9), 1231, **2021**.
17. AHMAD F., DRAZ M.U., CHANG W.-Y., YANG S.-C., SU L. More than the resource curse: Exploring the nexus of natural resource abundance and environmental quality in northwestern China. Resources Policy. **70**, 101902, **2021**.
18. HAN X., ZHAO Y., GAO X., JIANG S., LIN L., AN T. Virtual water output intensifies the water scarcity in Northwest China: Current situation, problem analysis and countermeasures. Science of the Total Environment. **765**, 144276, **2021**.
19. ZHAI M., HU R., WANG Y., JIANG S., WANG R., LI J., CHEN H., YANG Z., LÜ Q., QI T., SHI X. Mineral resource science in China: review and perspective. Geography and Sustainability. **2** (2), 107, **2021**.
20. JI W., YANG B., JIANG H., FENG B. Progresses of geological and mineral survey project in main metallogenic belts of Northwest China. Geological Survey of China. **4** (6), 1, **2017**.
21. ARISKIN A.A., PSHENITSYN I.V., DUBININA E.O., KOSSOVA S.A., SOBOLEV S.N. Sulfur isotope composition of olivine gabbronorites from a mineralized apophysis of the Yoko-Dovyren intrusion, Northern Transbaikalia, Russia. Petrology. **29**, 597, **2021**.
22. AO K., PIRAJNO F., XU Y., ZHANG S., SUN L., CONG Y., FAN J., YIN J., ZHU Y., WEI H. Study on the major minerals potential in China. Ore Geology Reviews. **127**, 103816, **2020**.
23. JIANG S., SU H., XIONG Y., LIU T., ZHU K., ZHANG L. Spatial-temporal distribution, geological characteristics and ore-formation controlling factors of major types of rare metal mineral deposits in China. Acta Geologica Sinica-English Edition. **94** (6), 1757, **2020**.
24. CHEN C., GU Y.-C., ZHANG D., WU T.-T., LI A., REN Y.-S., SHANG Q.-Q., ZHANG J., BIAN X.-F., SU F.,

YANG J.-L., SUN Q.-S., LI X.-H., LIU W.-Z., SUN Z.-M., ZHANG S., FENG Y.-H. Geology and mineralization of the Hongqiling large magmatic nickel-copper-cobalt deposit (22×10^4 t) in Jilin Province, China: A review. China Geology. **7** (4), 762, **2024**.
25. LI W., ZHANG Z., GAO Y., HONG J., CHEN B., ZHANG Z. Tectonic transformation of the Kunlun Paleo-Tethyan orogenic belt and related mineralization of critical mineral resources of nickel, cobalt, manganese and lithium. Geology in China. **49** (5), 1385, **2022**.
26. XU Y., HE F., ZHANG J. The problems of environmental geology and database for mining in Northwestern China. Northwestern Geology. **35**, 154, **2002**.
27. ZHANG X., CHENG B., CHEN X., LIANG C. High-resolution boundary refined convolutional neural network for automatic agricultural greenhouses extraction from GaoFen-2 satellite imageries. Remote Sensing. **13** (21), 4237, **2021**.
28. YANG A., ZHONG B., HU L., WU S., XU Z., WU H., WU J., GONG X., WANG H., LIU Q. Radiometric cross-calibration of the wide field view camera onboard GaoFen-6 in multispectral bands. Remote Sensing. **12** (6), 1037, **2020**.
29. DONG G. The political background of a pattern transformation in the Chinese system of science and technology during the 20th century. Cultures of Science. **5** (1), 16, **2022**.
30. LIU J., LIU R., TAN Y., LI F., WEN M., XI J. Development and application of geological survey information technology in CGS. Thai Geoscience Journal. **5** (7), 32, **2024**.
31. FU B., LIU Y., LI Y., WANG C., LI C., JIANG W., HUA T., ZHAO W. The research priorities of Resources and Environmental Sciences. Geography and Sustainability. **2** (2), 87, **2021**.
32. LI C., ZHOU Y., ZHENG X., ZHANG Z., JIANG L., LI Z., WANG P., LI J., XU S., WANG Z. Tracing the footsteps of open research data in China. Learned Publishing. **35** (1), 46, **2022**.
33. FAN J., ZHANG X., CHEN Y., SUN C. Classification of hyperspectral image by a preprocessing method based relation network. International Journal of Remote Sensing. **44** (22), 6929, **2023**.
34. WANG W., ZHANG P.Y., WANG X. An approach for automatic preprocessing of high-resolution remote sensing data and vegetation extraction based on ENVI/IDL. Journal of Hunan City University (Natural Science). **29** (2), 45, **2020**.
35. ZHANG C., LUO L., XU W., LEDWITH V. Use of local Moran's I and GIS to identify pollution hotspots of Pb in urban soils of Galway, Ireland. Science of the Total Environment. **398** (1), 212, **2008**.
36. CHEN Y. Spatial autocorrelation equation based on Moran's index. Scientific Reports. **13** (1), 19296, **2023**.
37. LANORTE A., NOLÈ G., CILLIS G. Application of Getis-Ord correlation index (Gi) for burned area detection improvement in Mediterranean ecosystems (Southern Italy and Sardinia) using Sentinel-2 data. Remote Sensing. **16** (16), 2943, **2024**.
38. LIU W., MA L., SMANOV Z., SAMARKHANOV K., ABUDUWAILI J. Clarifying soil texture and salinity using local spatial statistics (Getis-Ord Gi* and Moran's I) in Kazakh-Uzbekistan border area, Central Asia. Agronomy. **12** (2), 332, **2022**.
39. MAUS V., GILJUM S., GUTSCHHOFER J., DA SILVA D.M., PROBST M., GASS S.L., LUCKENEDER S., LIEBER M., MCCALLUM I. A global-scale data set of mining areas. Scientific Data. **7** (1), 289, **2020**.
40. MAUS V., CÂMARA G., CARTAXO R., SANCHEZ A., RAMOS F.M., DE QUEIROZ G.R. A time-weighted dynamic time warping method for land-use and land-cover mapping. IEEE Journal of Selected Topics in Applied Earth Observations and Remote Sensing. **9** (8), 3729, **2016**.
41. TANG L., WERNER T.T. Global mining footprint mapped from high-resolution satellite imagery. Communications Earth & Environment. **4** (1), 134, **2023**.
42. LIANG T., WERNER T.T., XIE H., YANG X., SHI Z. A global-scale spatial assessment and geodatabase of mine areas. Global and Planetary Change. **204**, 103578, **2021**.
43. CABERNARD L., PFISTER S. Hotspots of mining-related biodiversity loss in global supply chains and the potential for reduction through renewable electricity. Environmental Science & Technology. **56** (22), 16357, **2022**.
44. LLOYD T.J., OLIVEIRA U., SOARES-FILHO B.S., FULLER R.A., BUTT N., ASCHER J.S., BARBOSA J.P.P., BATISTA J.A.N., BRESCOVIT A.D., DE CARVALHO C.J.B., DE MARCO P., FERRO V.G., LEITE F.S.F., LÖWENBERG-NETO P., PAGLIA A.P., DE REZENDE D.T., SANTOS A.J., SILVA D.P., VASCONCELOS M.F., LAURA J. Multiple facets of biodiversity are threatened by mining-induced land-use change in the Brazilian Amazon. Diversity and Distributions. **29** (9), 1190, **2023**.
45. LU Y., HAN F., LIU Q., WANG Z., WANG T., YANG Z. Evaluation of potential for nature-based recreation in the Qinghai-Tibet Plateau: A spatial-temporal perspective. International Journal of Environmental Research and Public Health. **19**, 5753, **2022**.
46. LI T., JOHANSEN K., MCCABE M.F. A machine learning approach for identifying and delineating agricultural fields and their multi-temporal dynamics using three decades of Landsat data. ISPRS Journal of Photogrammetry and Remote Sensing. **186**, 83, **2022**.
47. VASUKI Y., YU L., HOLDEN E.-J., KOVESI P., WEDGE D., GRIGG A.H. The spatial-temporal patterns of land cover changes due to mining activities in the Darling Range, Western Australia: A visual analytics approach. Ore Geology Reviews. **108**, 23, **2019**.
48. MUKHERJEE J., MUKHERJEE J., CHAKRAVARTY D., AIKAT S. A novel index to detect opencast coal mine areas from Landsat 8 OLI/TIRS. IEEE Journal of Selected Topics in Applied Earth Observations and Remote Sensing. **12** (3), 891, **2019**.
49. National Bureau of Statistics of China, China Statistical Yearbook, 2023ed.; China Statistics Press: Beijing, China, pp. 229, **2023**.
50. YU L., XU Y., XUE Y., LI X., CHENG Y., LIU X., PORWAL A., HOLDEN E.J., YANG J., GONG P. Monitoring surface mining belts using multiple remote sensing datasets: A global perspective. Ore Geology Reviews. **101**, 675, **2018**.